# CNS origins of the sympathetic nervous system outflow to brown adipose tissue

MARYAM BAMSHAD,[1] C. KAY SONG,[2] AND TIMOTHY J. BARTNESS[1,2]
[1]*Neuropsychology and Behavioral Neurosciences Program, Department of Psychology; and*
[2]*Neurobiology Program, Department of Biology, Georgia State University, Atlanta, Georgia 30303*

**Bamshad, Maryam, C. Kay Song, and Timothy J. Bartness.** CNS origins of the sympathetic nervous system outflow to brown adipose tissue. *Am. J. Physiol.* 276 (*Regulatory Integrative Comp. Physiol.* 45): R1569–R1578, 1999.—Brown adipose tissue (BAT) plays a critical role in cold- and diet-induced thermogenesis. Although BAT is densely innervated by the sympathetic nervous system (SNS), little is known about the central nervous system (CNS) origins of this innervation. The purpose of the present experiment was to determine the neuroanatomic chain of functionally connected neurons from the CNS to BAT. A transneuronal viral tract tracer, Bartha's K strain of the pseudorabies virus (PRV), was injected into the interscapular BAT of Siberian hamsters. The animals were killed 4 and 6 days postinjection, and the infected neurons were visualized by immunocytochemistry. PRV-infected neurons were found in the spinal cord, brain stem, midbrain, and forebrain. The intensity of labeled neurons in the forebrain varied from heavy infections in the medial preoptic area and paraventricular hypothalamic nucleus to few infections in the ventromedial hypothalamic nucleus, with moderate infections in the suprachiasmatic and lateral hypothalamic nuclei. These results define the SNS outflow from the brain to BAT for the first time in any species.

pseudorabies virus; thermogenesis; obesity; autonomic nervous system; tract tracing; central nervous system

BROWN ADIPOSE TISSUE (BAT) plays a critical role in the increased heat production occurring with cold exposure (for review see Ref. 19) or overeating (for review see Ref. 41). BAT receives a dense innervation by the sympathetic nervous system (SNS; for review see Ref. 20), and this innervation plays an important role in heat production by BAT. The BAT pad receiving the most attention is interscapular BAT (IBAT) because of its size, accessibility (8), and clear SNS innervation [5 bilateral nerve bundles (i.e., intercostal nerves) going to each pad] (12).

Injections of the retrograde tract tracer horseradish peroxidase into laboratory rat IBAT pads labeled the proximate neuroanatomic distribution of the postganglionic neurons that innervate this BAT depot (49). The central nervous system (CNS) sites that innervate the preganglionic sympathetic neurons in the spinal cord that, in turn, project to these postganglionic neurons remain to be determined neuroanatomically, however. The location of these sites has been inferred using lesions or electrical or chemical stimulation of the CNS followed by assessment of changes in IBAT morphology, biochemistry, and electrophysiology (for review see Ref. 20). For example, the ventromedial hypothalamus (VMH) has been implicated in the control of BAT thermogenesis, because electrical or chemical stimulation of the VMH results in morphological and biochemical changes in IBAT as well as changes in the firing rates of the SNS intercostal nerves innervating IBAT (e.g., Ref. 4; 2, 5, 18, 23, 35, 40, 46, 54, 56–58). Complementary lesion studies appear to implicate further the role of VMH in BAT thermogenesis (e.g., Ref. 14; 21, 22, 32, 38, 43, 45, 48, 60, 61). The interpretation of these VMH stimulation or lesion data and of stimulation and lesion data of other brain sites (e.g., Ref. 6; 3, 10, 13, 15, 25, 50) on BAT thermogenesis can be difficult because of the inherent problems of confining the stimulation or lesion to these brain targets of interest. Although several brain regions have been implicated in the regulation of BAT function as a result of these stimulation and lesion studies, no neuroanatomic data exist for the origins of the SNS outflow from brain to BAT.

The present experiment was designed to answer the question: what is the neuroanatomic chain of functionally connected neurons from the CNS to BAT? This was accomplished with the use of a transneuronal viral tract tracer, Bartha's K strain of the pseudorabies virus (PRV). A similar strategy was successful in defining the CNS origins of the SNS outflow from brain to white adipose tissue (WAT) recently (7).

## METHODS

*Animals.* Adult male Siberian hamsters (*Phodopus sungorus sungorus*) were obtained from a breeding colony maintained at Georgia State University. The hamsters were initially group-housed (10–12/cage) in polyvinyl cages (48 × 27 × 15 cm) and kept in a light-dark (LD) cycle that simulated long-day, summerlike conditions (16:8 LD with lights on at 0300). Purina Rodent Chow (no. 5001) and water were available ad libitum.

*Surgical procedures.* Eight hamsters were anesthetized with pentobarbital sodium (50 mg/kg), and the IBAT was exposed. An attenuated strain of the Bartha's $gC^{Ka}$ PRV was injected into IBAT. The virus initially was supplied by Dr. Arthur Loewy (Washington Univ., St. Louis, MO) and then by Dr. Teryl Frey (Georgia State Univ.). PRV ($10^8$ plaque-forming units/ml) was injected unilaterally into the right IBAT pad in 120-nl volumes into five areas across its length ($n$ = 8 hamsters). All injections were made in the morning between 0900 and 1100 under a fume hood. The time course for PRV infection rate was determined by killing the animals at various intervals after PRV injections. Our previous PRV study in WAT of Siberian hamsters (7) showed that infection in brain stem neurons could be detected 96 h after PRV injection into this tissue. The infection reaches the hypothalamus and extends into the forebrain areas by 144 h after PRV

The costs of publication of this article were defrayed in part by the payment of page charges. The article must therefore be hereby marked "*advertisement*" in accordance with 18 U.S.C. Section 1734 solely to indicate this fact.

 

injections. Therefore, to induce infections extending into the forebrain areas, hamsters were killed at intervals of 96 h, or 4 days ($n$ = 4 hamsters), and 144 h, or 6 days ($n$ = 4 hamsters). Animals were perfused intracardially with 4% paraformaldehyde in the morning between 0900 and 1100.

*Immunocytochemical procedures*. The brains were postfixed overnight in 4% paraformaldehyde followed by overnight incubation in 25% sucrose. Brains were cut coronally into 50-μm-thick sections on a freezing microtome and stored in five vials of 0.1 M sodium phosphate buffer with 0.1% sodium azide. One of every five sets of stored sections was incubated in a pig polyclonal antibody to PRV (donated by Dr. Kenneth Platt, Iowa State Univ.) overnight at room temperature. The PRV antibody was diluted 1:30,000 in a buffer containing 2% normal rabbit serum and 0.3% Triton X-100. The sections were then incubated in biotinylated rabbit anti-pig secondary antibody (Sigma) at a 1:100 dilution for 2 h at room temperature. Next, the sections were incubated in the avidin-biotin horseradish peroxidase complex (Vectastain ABC Elite kit; Vector Laboratories, Burlingame, CA) at a 1:200 dilution for 1 h at room temperature. PRV-infected neurons were visualized with 3,3′-diaminobenzidine. The sections were cleared with xylene and placed under coverslips with DPX. The specificity of the immunocytochemical staining for the pig anti-PRV antibody used in this study has been validated previously (51).

The animals that had PRV infections in the brain stem and forebrain neurons were checked for signs of lysis of the infected neurons in the spinal cord. The spinal cords were removed from the infected animals killed on *day 6*, the longest postinjection interval. The cords were postfixed overnight in 4% paraformaldehyde followed by overnight incubation in 25% sucrose. The entire length of the spinal cord, including all sections of the cervical, thoracic, and lumbar regions, was cut coronally into 50-μm-thick sections on a freezing microtome. The sections were stored in 0.1 M sodium phosphate buffer with 0.1% sodium azide. They were processed immunocytochemically following the same procedure as described above for brain sections.

*Histological quantification*. The PRV-labeled neurons in brain sections were localized and quantified using Image Tracer software (Translational Technology) and a stage-mounted position transducer system (MD3 Microscope Digitizer, Minnesota Datametrics). Camera lucida pictures of each brain section, stained with cresyl violet, were drawn and scanned into the computer. A digital image of each drawing was projected onto the computer screen with the Image Tracer program. The image of each brain section was registered with the same section on the microscope stage with the use of the stage transducers. For all animals, the position of PRV-labeled neurons on each brain section was visualized with the microscope and marked in the exact position on the computerized image of that section. The number of marked PRV-labeled neurons was counted in each nucleus for each animal. The absolute number of infected neurons was combined for ipsilateral and contralateral sides of the injection site for each brain region and analyzed statistically using a two-way ANOVA (brain site × time postinjection). Mean percentages of total infected cells for the brain stem, midbrain, and forebrain areas were calculated. Post hoc comparisons were done using Duncan's new multiple range tests (29).

## RESULTS

Of eight hamsters injected with PRV, five became infected. One of the animals killed on *day 4* and two of the animals killed on *day 6* had no infections. There was no sign of illness in the infected animals with exception of slight weight loss in *day 6* animals.

*Spinal cord*. Quantification of virus distribution within the spinal cord was not conducted; however, the entire length of the spinal cords of *day 6* animals, those with the longest postinjection survival period, were inspected microscopically to screen for lysis of the infected cells. In addition, the presence of infected cells in the ventral horns also was determined, because such infections would indicate spread of the virus from the IBAT pad to underlying musculature. The spinal cords were sectioned coronally, and the cervical, thoracic, and lumbar regions were not marked before cord removal; thus it was not possible to determine the exact level of the cord at which neurons were infected. Lysis did not occur in any of the infected neurons, nor were there any cases of infected cells in the ventral horns. Infected neurons were seen only in a well-defined cluster located in the intermediolateral cell group and the central autonomic nucleus of the spinal cord ipsilateral to the injection site (i.e., the SNS preganglionics; Fig. 1).

*Data presentation*. The distribution of infected neurons is presented schematically in Fig. 2. These seven levels of the neuroaxis were chosen because the densest infections were seen at these levels. Figure 3 is composed of representative microphotographs from infected animals at low and high magnifications. The letter-number designations correspond as closely as possible to the letter designations for each level of the neuroaxis in Fig. 2.

*Brain stem*. Figures 2, *A–C*, and 3, *A–C*, show the distribution of and examples of, respectively, some of the infected neurons in brain stem at *day 6* after injection of the virus into IBAT. At this level of the neural axis, the infection was bilateral and uniform.

In *day 4* animals, the virus invaded most of the ventrally located nuclei in the brain stem. Labeling was sparse among dorsally located nuclei. For example, among dorsally located nuclei, only a few infected neurons were found throughout the rostrocaudal extent of the dorsal aspects of the nucleus of the solitary

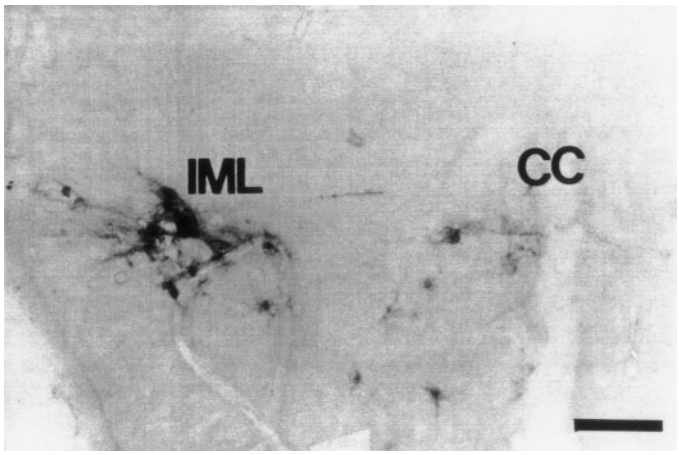


Fig. 1. Photomicrograph illustrating distribution of pseudorabies virus (PRV)-labeled cells in spinal cord of *day 6* hamster (longest postinjection period). Bar = 200 μm. CC, central canal; IML, intermediolateral nucleus.

tract (Sol) and the medial aspects of the medial vestibular nucleus (MVe). At the most caudal levels of the brain stem (bregma = −14.30 to −13.30 mm), infection was found in low levels in the neurons of the lateral reticular nucleus and medullary reticular nuclei, dorsal and ventral aspects. At this level, a few infected neurons were found in the raphe pallidus nucleus (Rpa). At the level of the C1 epinephrine cells (C1) and rostroventrolateral reticular nucleus (RVL) regions (bregma = −13.30 to −12.72 mm), intense labeling was seen in the intermediate reticular nucleus (IRt), with moderate labeling of the C1/RVL neurons. Some of the neurons of the parvocellular reticular nucleus also were labeled. More rostrally, the infection in the IRt and C1/RVL regions had intensified. At the level of the MVe, neurons were heavily infected in the C1/RVL region, the caudal raphe, including the Rpa and raphe obscurus nucleus (ROb), and all aspects of the gigantocellular reticular nucleus (Gi). At the level of the facial nucleus, PRV infected the norepinephrine cells (A5) region. The caudal raphe nuclei, the Gi, the lateral paragigantocellular nucleus (LPGi), and the raphe magnus remained heavily infected at this level.

In *day 6* animals, the pattern of distribution of infected neurons was quite similar to that of *day 4* animals; the infection was contained within the same nuclei. In the majority of nuclei examined, however, intensity of infection was much more severe in *day 6* vs. *day 4* animals. For example, the virus that had infected the dorsal aspects of the Sol in *day 4* animals was transmitted to the lateral and ventral portions of the Sol by *day 6*. In some regions, such as the caudal raphe (ROb/Rpa), the virus infected neurons in the entire rostrocaudal extent of the nuclei.

Table 1, which shows the mean ± SE of infected neurons in each brain region across days, has been provided to illustrate the difference in degree of infection between *day 4* and *day 6* animals. The average number of infected neurons combined for all brain stem regions was significantly higher in *day 6* than in *day 4* animals ($F = 30.10$, $P < 0.001$). The difference in average number of infected neurons among brain regions across the two postinjection intervals approached significance ($P = 0.07$). The mean percentage of total infected cells across all brain stem regions in *day 6* hamsters showed that 20.9% of total infected cells were found in the IRt. The A5 had 15.2%, the Rpa/ROb had 12.2%, the LPGi had 11.0%, and the C1 had 10.3% of the total number of infected cells. The lowest mean percentage of total infected cells was in the Gi at 4.3%.

*Midbrain*. Figures 2*D* and 3*D* show the distribution of and examples of, respectively, some of the infected neurons in brain stem at *day 6* after injection of the virus into IBAT. The infection also was bilateral and uniform at this level of the neural axis. The most heavily infected area in the midbrain was the central gray (CG). Infections throughout the rostrocaudal extent of the CG were found in hamsters killed 4 days after PRV injections. The most intense labeling was found in the caudal regions, at the level of the pyramidal tract (Py) in the ventral portions of the CG. More rostrally, at the level of pontine nuclei (Pn; bregma = −8.00 to −7.64 mm), PRV-infected neurons were seen in lateral and ventral portions of the central gray (CGLV) and surrounding areas and posterior to the dorsal raphe nucleus (DR). A few scattered PRV neurons were found in the lateral dorsal central gray (CGLD), but none were found in the dorsal central gray (CGD) or medial central gray.

The PRV was transmitted more extensively by the *day 6* postinjection interval. As in *day 4* animals, hamsters killed on *day 6* had the majority of their PRV-infected neurons in the ventral portion of the CG at the level of Py. A few infected neurons had invaded the DR. More rostrally, throughout the Pn sections, intense labeling was seen in the CGLV. In *day 6* animals, more infected neurons were found in the CGLD, and a few were seen in the CGD portion. At the level of the ventral tegmental area, a few PRV-infected neurons also were found in the CG and CGD areas.

*Forebrain*. Figures 2, *E–G*, and 3, *E–G*, show the distribution of and examples of, respectively, some of the infected neurons in the forebrain at *day 6* after injection of the virus into IBAT. Infections were bilateral at this level of the neural axis, but a greater density of labeling was seen ipsilateral to the injection site. The average number of infected neurons at each site is shown in Table 1. As in the brain stem and midbrain, with an increase in postinjection interval from 4 to 6 days, the PRV infection significantly intensified in each nucleus ($F = 15.57$, $P < 0.001$) but remained confined to the same regions.

In *day 4* animals, labeled neurons were found in the lateral hypothalamus (LH) and zona incerta (ZI) at the level of the VMH. A few infected neurons also were seen in the dorsal hypothalamic area. In only one animal, two infected neurons were found at the border of the VMH. Rostrally, at the retrochiasmatic area, the majority of infected cells were in the medial parvicellular and ventral aspects of the paraventricular nucleus (PVN); however, the infection also had extended to the borders of, and slightly within, the magnocellular portion. At the level of the suprachiasmatic nucleus (SCN), the anterior parvicellular PVN and medial preoptic area (MPA) were the only regions labeled. A few infected cells were seen at the lateral border of the SCN. No infected neurons were seen in the more rostral sections of the forebrain.

In *day 6* animals, the infection intensified within the same nuclei. For example, at the level of the VMH, many more infected neurons appeared across the entire LH and ZI. The infection also penetrated the VMH. A similar situation was observed in the SCN and all areas of the PVN. PRV-infected neurons were seen throughout the lateral SCN and were visible in the medial aspects of this nucleus. Both parvicellular and magnocellular portions of the PVN were heavily labeled with PRV. In addition, the virus was transmitted to more rostral sections of the forebrain and infected the lateral and ventral septum as well as the bed nucleus of the stria terminalis (BNST). There was a significant difference in the total number of infected neurons among

forebrain regions ($F = 4.37$, $P < 0.05$), with significantly larger numbers of infected neurons in magnocellular and parvicellular portions of the PVN (combined) and in the MPA ($P < 0.05$). Specifically, 6 days after PRV injections, 38.7% and 32.3% of the total number of infected neurons were found in the PVN and the MPA, respectively. In contrast, only 1.6% of the total number of infected neurons was found in the VMH. Moderate PRV infection was seen in the LH (9.5%) and in the SCN (8.8%). The areas with the lowest percentage of total infected cells were the BNST (4.2%) and the lateral septum (LS; 2.2%).

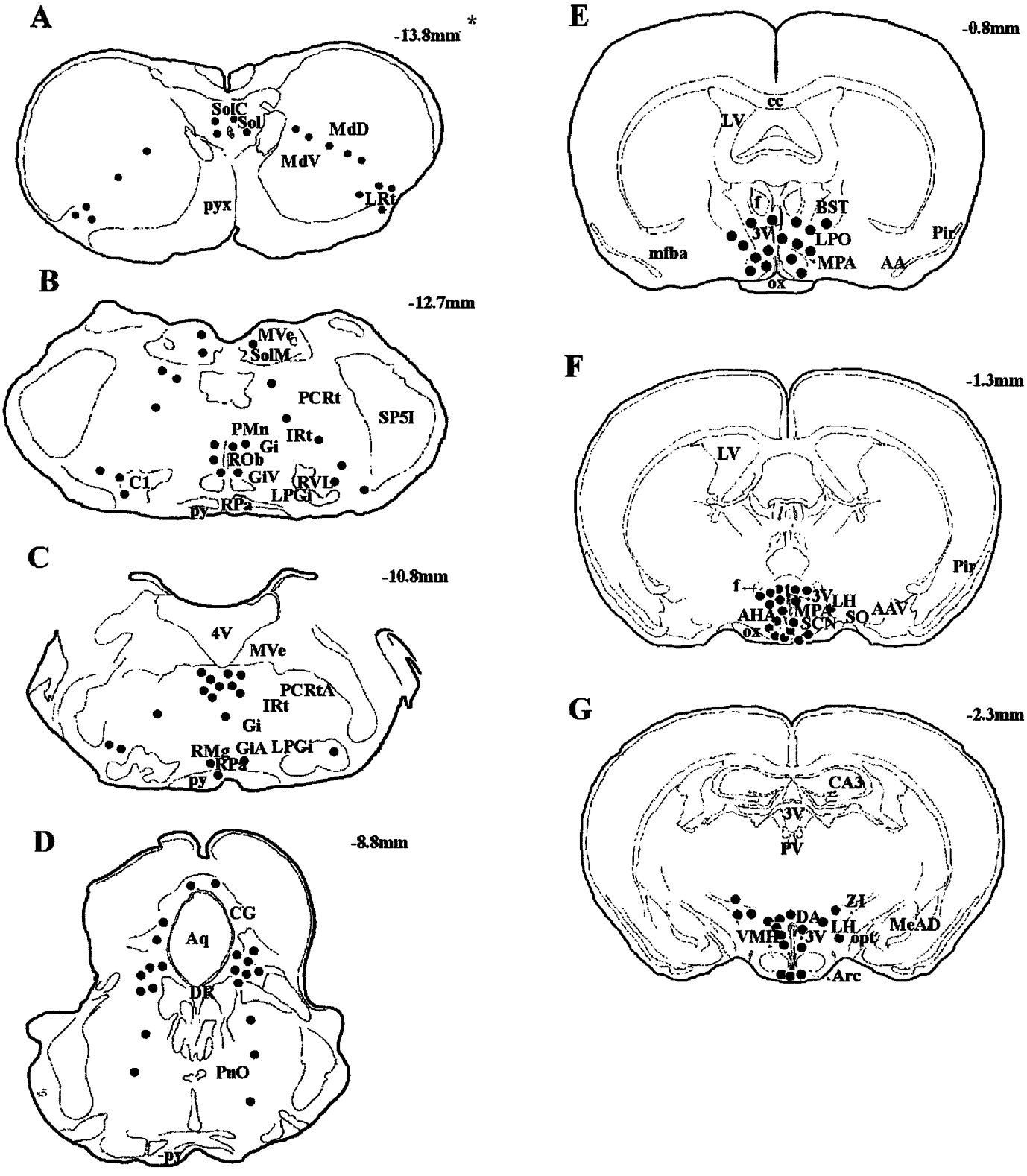

## DISCUSSION

These results provide the first neuroanatomic description of the SNS outflow from the brain to BAT in any species. The pattern of labeling observed in the present study after PRV was injected into IBAT resembled the pattern of labeling seen after PRV injections into WAT of Siberian hamsters and laboratory rats (7) and of labeling seen after PRV injections into the adrenal medulla of laboratory rats (53) or Siberian hamsters (unpublished observations). Collectively, these suggest that some of the labeling seen after injections of the virus into IBAT labeled part of the general SNS outflow from the brain to the periphery (52). We found, however, that although it was similar to the labeling after PRV injections into WAT or the adrenal medulla, there were some differences in the degree of labeling of certain brain structures. Specifically, higher percentages of cells were infected in the A5 and caudal raphe (ROb and Rpa collectively, Table 1) regions of the brain stem after BAT (15.2% and 12.2%, respectively) vs. WAT (4% and 5%, respectively) (7) injections of the virus. There also were more infected neurons in the LH and the BNST in animals injected with PRV into IBAT than there were in animals injected with the virus into WAT (7).

Previous attempts to identify the CNS origins of the SNS innervation of IBAT used nonneuroanatomic techniques (i.e., stimulation or lesions) and measured changes in IBAT morphology, biochemistry, or neurophysiology. The VMH has been implicated in most of these studies (for review see Ref. 20), yet we found little or no neural connections between the VMH and IBAT using this transneuronal viral tract tracer (see Table 1 and Fig. 1*G*). One possible reason for the discrepancy between the results of the nonneuroanatomic studies and those of the present neuroanatomic study is that the targeted stimulation or destruction of the VMH secondarily affected the caudally projecting neurons of the hypothalamic PVN that course near and around the VMH (24, 28, 33). When these PVN neurons are stimulated or destroyed more directly, BAT physiological, biochemical, and/or morphological thermal responses are affected (e.g., Ref. 9; 3, 10, 13). Therefore, previous attempts to affect IBAT thermogenesis through manipulations of the VMH may have altered these caudally projecting PVN neurons known to make direct connections with the spinal preganglionics (for review see Ref. 31). In this manner, BAT thermogenesis may ultimately have been affected.

Concerning the infections seen in the magnocellular region of the PVN, it should be noted that we believe this labeling was not a result of vascular transport of PRV to, for example, the posterior pituitary. This interpretation is based on the inability of PRV injected directly into peripheral venous or arterial blood to induce CNS infections, even at long postinjection survival times (30). Rather, it seems more likely that the scattered spinally projecting parvicellular neurons located within the magnocellular area (36) as well as the merging of the dorsal and ventral parvicellular spinally projecting areas more caudally within the hamster PVN (36) are the origins of the infections seen in the magnocellular PVN in the present study. The magnocellular neuronal infections seen in the present study and the lesser infections seen in other studies wherein PRV was injected into peripheral tissues (52, 53), including our own study after injections of virus into WAT (7), could be explained by transsynaptic spread of PRV within and between the nucleus subdivisions.

Innervation of BAT by the SCN has been suggested by an increase in IBAT thermogenesis after electrical stimulation of the retinohypothalamic tract that innervates the SCN (1) or by glutamate injections directly into the SCN (6). In the present study, a substantial number of infected neurons were visualized in the SCN after injection of PRV into IBAT. It is tempting to speculate that the SCN-BAT connection may be involved in the circadian timing of torpor bouts in Siberian hamsters, because SCN lesions block the expression of the torpor-associated rhythmic daily decreases in body temperature in this species (42).

We also found extensive labeling of PRV-infected neurons in the MPA. These data may help explain why electrical (59) or chemical (11) stimulation of the MPA increases IBAT thermogenesis and the firing rate of the sympathetic nerves that innervate IBAT (11, 59), respectively. The roles of the MPA and the SCN in BAT thermogenesis, however, are not well understood.

Fig. 2. Schematic diagrams showing distribution of PRV-labeled cells in cross sections through brain from caudal to rostral (*A*–*G*) levels in Siberian hamsters 6 days after PRV injection into right interscapular brown adipose tissue (IBAT). Each symbol represents 1–40 infected neurons. *Bregma measurements copied from rat atlas (39). 3V, 3rd ventricle; 4V, 4th ventricle; 7, facial nucleus; A5, A5 norepinephrine cells; AAV, anterior amygdaloid area, ventral part; AHA, anterior hypothalamic area; Aq, aqueduct; Arc, arcuate; BST, bed nucleus of the stria terminalis; C1, C1 epinephrine cells; CA3, CA3 of Ammon's horn; CC, central canal; cc, corpus callosum; CG, central gray; DA, dorsal hypothalamic area; DR, dorsal raphe nucleus; f, fornix; Gi, gigantocellular reticular nucleus; GiA, gigantocellular reticular nucleus, alpha part; GiV, gigantocellular reticular nucleus, ventral part; IRt, intermediate reticular nucleus; LH, lateral hypothalamic area; LPGi, lateral paragigantocellular nucleus; LPO, lateral preoptic area; LRt, lateral reticular nucleus; LV, lateral ventricle; MdD, medullary reticular nucleus, dorsal part; MdV, medullary reticular nucleus, ventral part; MeAD, medial amygdaloid nucleus, anterodorsal part; mfba, medial forebrain bundle; MPA, medial preoptic area; MVe, medial vestibular nucleus; opt, optic tract; ox, optic chiasm; PCRt, parvocellular reticular nucleus; PCRtA, parvocellular reticular nucleus, alpha part; Pir, piriform cortex; PnO, pontine reticular nucleus, oral part; PV, paraventricular thalamic nucleus; py, pyramidal tract; pyx, pyramidal decussation; RMg, raphe magnus nucleus; ROb, raphe obscurus nucleus; Rpa, raphe pallidus nucleus; RVL, rostroventrolateral reticular nucleus; SCh, suprachiasmatic nucleus; SO, supraoptic nucleus; Sol, nucleus of the solitary tract; SolC, nucleus of the solitary tract, commissural part; sp5, spinal trigeminal tract; Sp5I, spinal trigeminal nucleus, interpolar part; VMH, ventromedial hypothalamic nucleus; ZI, zona incerta.

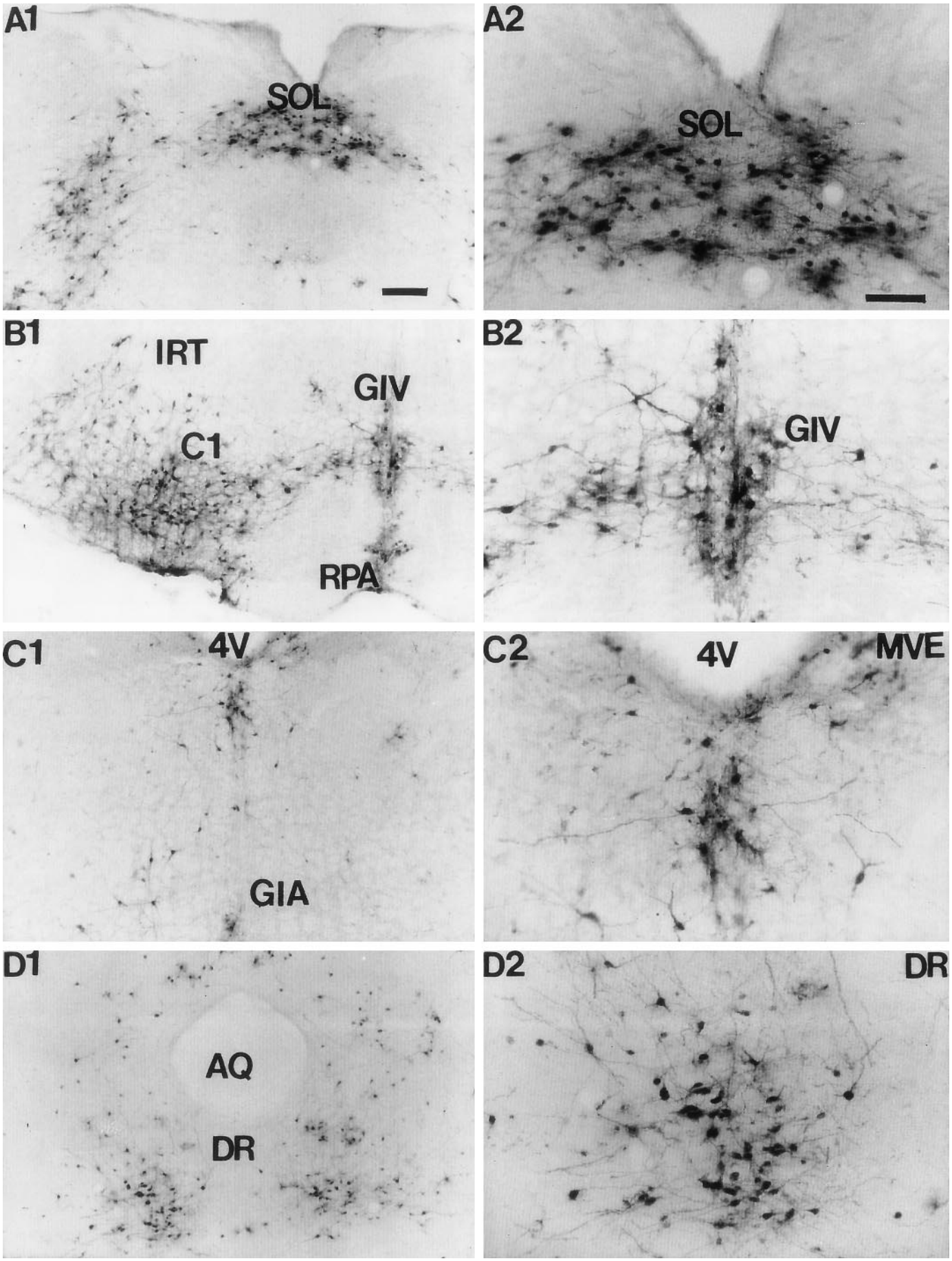

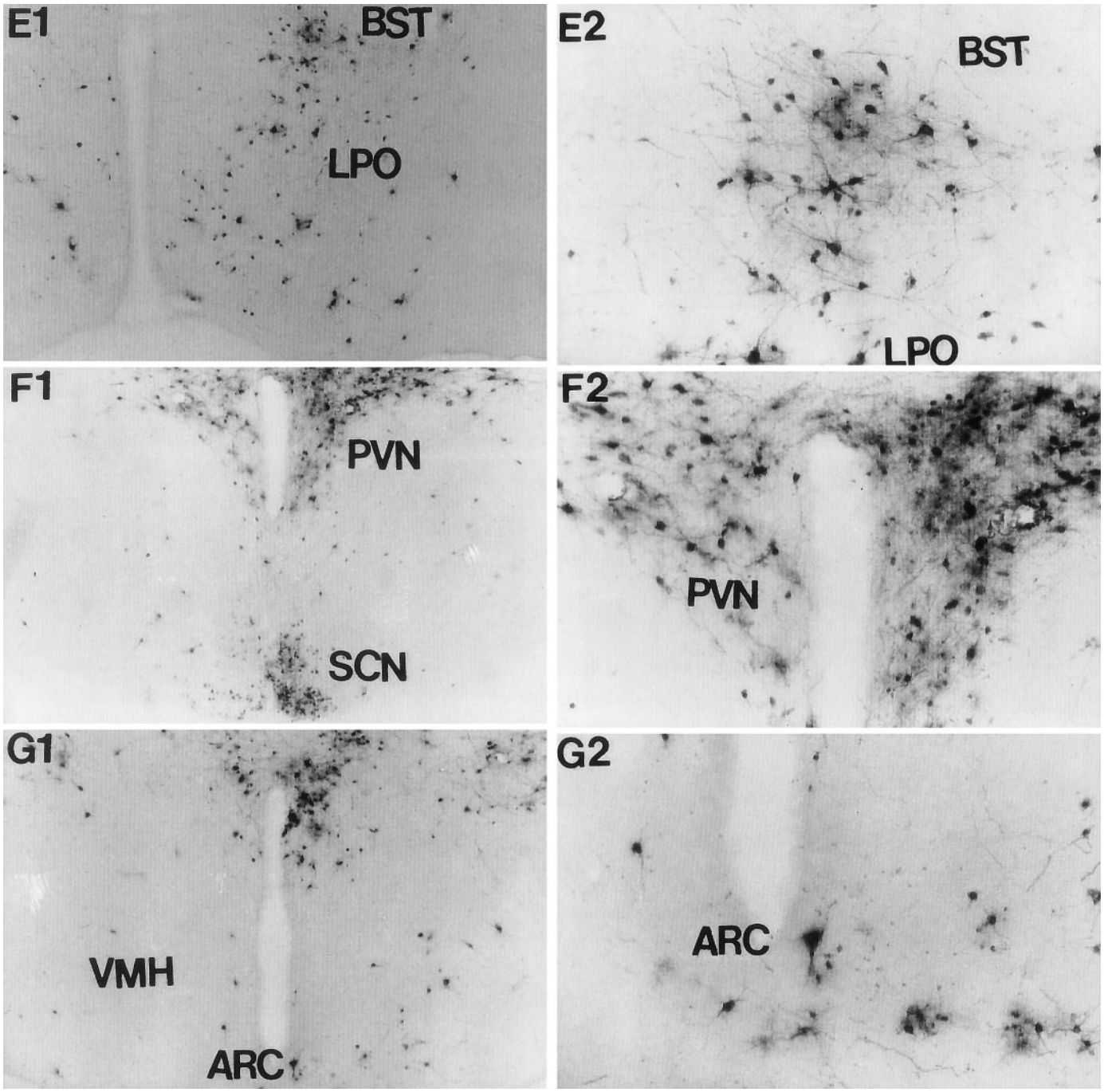


Fig. 3. Photomicrographs illustrating distribution of PRV-labeled cells in cross sections of brain from a representative Siberian hamster 6 days after PRV was injected into IBAT. Letters correspond to those for the schematic distribution analysis of the data shown in Fig. 2. *Left*: low-magnification photomicrographs. *Right*: higher magnification of selected portions of corresponding photomicrographs at *left*. 4V, fourth ventricle; AQ, aqueduct; ARC, arcuate nucleus; BST, bed nucleus of the stria terminalis; C1, C1 epinephrine cells; DR, dorsal raphe nucleus; GIA, gigantocellular reticulate nucleus, alpha part; GIV, gigantocellular reticular nucleus; IRT, intermediate reticular nucleus; LPO, lateral preoptic nucleus; MVE, medial vestibular nucleus; RPA, raphe pallidus nucleus; PVN, paraventricular hypothalamic nucleus; SCN, suprachiasmatic nucleus; SOL, nucleus of the solitary tract; VMH, ventromedial hypothalamus. Bar = 200 μm; 100 μm at higher magnification.

Although the pattern of infection in the present study after PRV injections into IBAT was more similar than different compared with the pattern after virus injections into the adrenal medulla of laboratory rats (52, 53), there were some notable differences, especially in the forebrain. These sites included the SCN and MPA as well as the LS and the BNST. These areas also were infected after PRV injections into WAT pads in Siberian hamsters and laboratory rats (7). One possible explanation for these differences may be that we used a longer

Table 1. *Average number of transneuronally labeled neurons in brain of Siberian hamsters after injection of PRV into IBAT*

| | Postinjection Intervals | |
|---|---|---|
| | 4 days ($n = 3$) | 6 days ($n = 2$) |
| Brain stem | | |
| Sol | 2.7 ± 2.7 | 107.0 ± 37.0 |
| ROb/Rpa | 79.0 ± 27.9 | 130.0 ± 11.0 |
| LRt | 2.0 ± 2.0 | 89.0 ± 17.0 |
| C1/RVL | 85.7 ± 36.2 | 109.5 ± 4.5 |
| IRt | 23.3 ± 21.4 | 222.5 ± 101.5 |
| LPGi | 55.7 ± 30.0 | 117.5 ± 63.5 |
| GiA | 6.0 ± 3.5 | 45.5 ± 14.5 |
| A5 | 32.3 ± 14.2 | 162.5 ± 8.5 |
| Midbrain | | |
| CG | 5.7 ± 3.2 | 43.5 ± 32.5 |
| Hypothalamus | | |
| VMH | 0.7 ± 0.7 | 13.5 ± 10.5 |
| Arc | 1.3 ± 0.7 | 22.5 ± 10.5 |
| PVN | 71.7 ± 47.5 | 322.5 ± 143.5 |
| SCN | 0.7 ± 0.7 | 73.5 ± 57.5 |
| LH | 6.0 ± 2.3 | 79.0 ± 56.0 |
| MPA | 1.3 ± 0.9 | 269.5 ± 175.5 |
| BNST | | 35.5 ± 23.5 |
| LS | | 18.0 ± 7.0 |

All values are means ± SE; $n$ = no. of rats. PRV, pseudorabies virus; IBAT, interscapular brown adipose tissue; Sol, nucleus of the solitary tract; ROb/Rpa, raphe obscurus nucleus/raphe pallidus nucleus; LRt, lateral reticular nucleus; C1/RVL, C1 epinephrine cells/rostroventrolateral reticular nucleus; IRt, intermediate reticular nucleus; LPGi, lateral paragigantocellular nucleus; GiA, gigantocellular reticular nucleus, alpha part; A5, norepinephrine cells; CG, central gray; VMH, ventromedial hypothalamic nucleus; Arc, arcuate; PVN, paraventricular hypothalamic nucleus; SCN, suprachiasmatic nucleus; LH, lateral hypothalamic area; MPA, medial preoptic area; BNST, bed nucleus of the stria terminalis; LS, lateral septum.

survival period after the virus was injected into WAT (7) and IBAT than was used in the studies wherein PRV was injected into the adrenal medulla (52, 53) (i.e., 6 vs. 4 days, respectively). We believe that this explanation fails to account for some of the differences in labeling, because the MPA was one of the more rostral forebrain structures labeled, yet it showed the second largest number of infected neurons across the neural axis 6 days post-PRV injection (Table 1).

In a previous study, PRV was injected into WAT of Siberian hamsters and laboratory rats (7). The distribution of infected neurons in the brain after PRV injections into BAT seen in the present study is quite similar to that found in WAT. Some differences do exist between the CNS infections for each type of adipose tissue, however. First, PRV infected the brain much faster after injections into BAT than it did after injections into WAT. Within 4 days after injections into BAT, PRV had spread into several areas in the forebrain, whereas after injections into WAT, it took 6 days before a similar pattern of labeling was seen. This most likely was a result of the shorter distance the virus traveled from the BAT pad than it did from the WAT pads (inguinal and epididymal) (7). Second, PRV infections in all brain regions examined were much heavier after injections into BAT than they were after injection into WAT (7). In addition, there were some differences between BAT- and WAT-injected animals in the number of cells labeled in some brain regions (i.e., greater infections in the A5 and caudal raphe nuclei, and LH and BNST in BAT vs. WAT). The functional significance of these differences remains to be determined (see *Perspectives*).

In conclusion, the results of the present study suggest that the general SNS outflow to the periphery (52) also is involved in the SNS innervation of BAT (specifically, IBAT). In addition, other CNS sites identified as being connected neuroanatomically to BAT, such as the BNST, SCN, MPA, and LS, also are parts of the SNS innervation of WAT (7).

## *Perspectives*

Our understanding of the central control of peripheral metabolism has been hampered by the inability to trace the chain of neurons originating in the brain and terminating in peripheral glands and organs. The use of transneuronal viral tract tracers, such as the PRV, permits the definition of neural circuits, such as those involved in the central control of peripheral metabolism, within the same animal. The work to date delineating the SNS innervation of a variety of peripheral tissues, including BAT (in the present study), WAT (7), the adrenal medulla (26, 52, 53), the kidney (47), and other peripheral tissues, such as the heart (26, 27, 55), suggests a general SNS outflow from the CNS to the periphery (52). A critical question is raised because of these similarities: how is this general SNS outflow from the brain to the periphery regulated under conditions where there are differential SNS drives on peripheral tissues? Moreover, given the present findings for BAT and our previous findings for WAT (7), a more specific question can be posited: how can there be both separate and simultaneous SNS drives to BAT and WAT? An example of the separate SNS control of these adipose tissues is starvation or severe food restriction. In these conditions of reduced caloric intake, the SNS drive to BAT, and consequently BAT thermogenesis, is decreased (44), and the SNS drive to WAT, and consequently WAT lipolytic activity, is increased (34). An example of the simultaneous SNS control of these adipose tissues is cold exposure. In this condition, the SNS drive to BAT, and consequently BAT thermogenesis, is increased (37, 62); the SNS drive to WAT, and consequently WAT lipolytic activity, is also increased (16, 17). Because of the relatively separate postganglionic SNS innervation of the epididymal and inguinal WAT pads, there may be an analogous separate postganglionic SNS innervation of WAT and BAT. Alternatively, the differences that are seen in the degree of innervation of WAT and BAT by the SNS in some CNS structures should not be overlooked as a means by which this differential control of the SNS drive on adipose tissues or, for that matter, other tissues and organs innervated by the SNS may be controlled.

The authors thank Drs. Arthur Loewy, Michael Stock, Patrick Card, and Frank Gordon for helpful discussions of these data. We also thank Dr. Kenneth Platt for providing the PRV antibody, Dr. Arthur Loewy for providing the initial supply of the virus, and Dr. Teryl Frey for providing the current supply of PRV. Finally, we thank Drs.

Arthur Loewy and Patrick Card for continued encouragement and suggestions.

This work was supported in part by National Institute of Diabetes and Digestive and Kidney Diseases Grant R01 DK-35254 and National Institute of Mental Health Research Scientist Development Award KO2 MH-00841.

Address for reprint requests and other correspondence: T. J. Bartness, Dept. of Biology, Georgia State Univ., Atlanta, GA 30303 (E-mail: bartness@gsu.edu).

Received 11 May 1998; accepted in final form 10 February 1999.

## REFERENCES

1. **Amir, S.** Retinohypothalmic tract stimulation activates thermogenesis in brown adipose tissue in the rat. *Brain Res*. 503: 163–166, 1989.
2. **Amir, S.** Intra-ventromedial hypothalamic injection of glutamate stimulates brown adipose tissue thermogenesis in the rat. *Brain Res*. 511: 341–344, 1990.
3. **Amir, S.** Stimulation of the paraventricular nucleus with glutamate activates interscapular brown adipose tissue thermogenesis in rats. *Brain Res*. 508: 152–155, 1990.
4. **Amir, S., M. Lagiorgia, and R. Pollock.** Intra-ventromedial hypothalamic injection of insulin suppresses brown fat thermogenesis in the anaesthetized rat. *Brain Res*. 480: 340–343, 1989.
5. **Amir, S., A. Schiavetto, and R. Pollock.** Insulin co-injection suppresses the thermogenic response to glutamate microinjection into the VMH in rats. *Brain Res*. 527: 326–329, 1990.
6. **Amir, S., P. Shizgal, and P.-P. Rompre.** Glutamate injection into the suprachiasmatic nucleus stimulates brown fat thermogenesis in the rat. *Brain Res*. 498: 140–144, 1989.
7. **Bamshad, M., V. T. Aoki, M. G. Adkison, W. S. Warren, and T. J. Bartness.** Central nervous system origins of the sympathetic nervous system outflow to white adipose tissue. *Am. J. Physiol*. 275 (*Regulatory Integrative Comp. Physiol*. 44): R291–R299, 1998.
8. **Bartness, T. J., and G. N. Wade.** Effects of interscapular brown adipose tissue denervation on estrogen-induced changes in food intake, body weight and energy metabolism. *Behav. Neurosci*. 98: 674–685, 1984.
9. **Coscina, D. V., J. W. Chambers, I. Park, S. Hogan, and J. Himms-Hagen.** Impaired diet-induced thermogenesis in brown adipose tissue from rats made obese with parasagittal hypothalamic knife-cuts. *Brain Res. Bull*. 14: 585–593, 1985.
10. **De Luca, B., M. Monda, S. Amaro, M. P. Pellicano, and L. A. Cioffi.** Lack of diet-induced thermogenesis following lesions of paraventricular nucleus in rats. *Physiol. Behav*. 46: 685–691, 1989.
11. **Egawa, M., H. Yoshimatsu, and G. A. Bray.** Preoptic area injection of corticotropin-releasing hormone stimulates sympathetic activity. *Am. J. Physiol*. 259 (*Regulatory Integrative Comp. Physiol*. 28): R799–R806, 1990.
12. **Foster, D. O., F. Depocas, and M. Zuker.** Heterogeneity of the sympathetic innervation of rat interscapular brown adipose tissue via intercostal nerves. *Can. J. Physiol. Pharmacol*. 60: 747–754, 1982.
13. **Freeman, P. H., and P. J. Wellman.** Brown adipose tissue thermogenesis induced by low level electrical stimulation of hypothalamus in rats. *Brain Res. Bull*. 18: 7–11, 1987.
14. **Fukushima, M., K. Tokunaga, J. Lupien, J. W. Kemnitz, and G. A. Bray.** Dynamic and static phases of obesity following lesions in PVN and VMH. *Am. J. Physiol*. 253 (*Regulatory Integrative Comp. Physiol*. 22): R523–R529, 1987.
15. **Fyda, D. M., K. E. Cooper, and W. L. Veale.** Modulation of brown adipose tissue-mediated thermogenesis by lesions to the nucleus tractus solitarius in the rat. *Brain Res*. 546: 203–210, 1991.
16. **Garofalo, M. A. R., I. C. Kettelhut, J. E. S. Roselino, and R. H. Migliorini.** Effect of acute cold exposure on norepinephrine turnover rates in rat white adipose tissue. *J. Auton. Nerv. Syst*. 60: 206–208, 1996.
17. **Gilgen, A., and R. P. Maickel.** Essential role of catecholamines in the mobilization of free fatty acids and glucose after exposure to cold. *Life Sci*. 12: 709–715, 1962.
18. **Halvorson, I., L. Gregor, and J. A. Thornhill.** Brown adipose tissue thermogenesis is activated by electrical and chemical (L-glutamate) stimulation of the ventromedial hypothalamic nucleus in cold-acclimated rats. *Brain Res*. 522: 76–82, 1990.
19. **Heldmaier, G., S. Klaus, H. Wiesinger, U. Friedrichs, and M. Wenzel.** Cold acclimation and thermogenesis. In: *Living in the Cold*, edited by A. Malan and B. Canguilhem. Montrouge, France: Libbey Eurotext, 1989, vol. 2, p. 347–358.
20. **Himms-Hagen, J.** Neural control of brown adipose tissue thermogenesis, hypertrophy, and atrophy. *Front. Neuroendocrinol*. 12: 38–93, 1991.
21. **Hogan, S., D. V. Coscina, and J. Himms-Hagen.** Brown adipose tissue of rats with obesity-inducing ventromedial hypothalamic lesions. *Am. J. Physiol*. 243 (*Endocrinol. Metab*. 6): E338–E344, 1982.
22. **Hogan, S., J. Himms-Hagen, and D. V. Coscina.** Lack of diet-induced thermogenesis in brown adipose tissue of obese medial hypothalamic-lesioned rats. *Physiol. Behav*. 35: 287–294, 1985.
23. **Holt, S. J., H. V. Wheal, and D. A. York.** Hypothalamic control of brown adipose tissue in Zucker lean and obese rats. Effect of electrical stimulation of the ventromedial nucleus and other hypothalamic centres. *Brain Res*. 405: 227–233, 1987.
24. **Hosoya, Y., Y. Sugiura, N. Okada, A. D. Loewy, and K. Kohno.** Descending input from the hypothalamic paraventricular neurons to sympathetic preganglionic neurons in the rat. *Exp. Brain Res*. 85: 10–20, 1991.
25. **Imai-Matsumura, K., and T. Nakayama.** The central efferent mechanism of brown adipose tissue thermogenesis induced by preoptic cooling. *Can. J. Physiol. Pharmacol*. 65: 1299–1303, 1987.
26. **Jansen, A. S. P., X. V. Nguyen, V. Karpitskiy, T. C. Mettenleiter, and A. D. Loewy.** Central command neurons of the sympathetic nervous system: basis of the fight-or-flight response. *Science* 270: 644–646, 1995.
27. **Jansen, A. S. P., M. W. Wessendorf, and A. D. Loewy.** Transneuronal labeling of CNS neuropeptide and monoamine neurons after pseudorabies virus injections into the stellate ganglion. *Brain Res*. 683: 1–24, 1995.
28. **Kirchgessner, A. L., and A. Sclafani.** Histochemical identification of a PVN-hindbrain feeding pathway. *Physiol. Behav*. 42: 529–543, 1988.
29. **Kirk, R. E.** *Experimental Design: Procedures for the Behavioral Sciences*. Belmont, CA: Brooks/Cole, 1968.
30. **Larsen, P. J., L. W. Enquist, and J. P. Card.** Characterization of the multisynaptic neuronal control of the rat pineal gland using viral transneuronal tracing. *Eur. J. Neurosci*. 10: 128–145, 1998.
31. **Loewy, A. D.** Central autonomic pathways. In: *Central Regulation of Autonomic Functions*, edited by A. D. Loewy and K. M. Spyer. New York: Oxford Univ. Press, 1990, p. 88–103.
32. **Luboshitzky, R., L. L. Bernardis, J. K. Goldman, and M. Kodis.** Brown adipose tissue metabolism in hypothalamic-obese rats. *Metabolism* 32: 108–113, 1983.
33. **Luiten, P. G. M., G. J. ter Horst, H. Karst, and A. B. Steffens.** The course of paraventricular hypothalamic efferents to autonomic structures in medulla and spinal cord. *Brain Res*. 329: 374–378, 1985.
34. **Migliorini, R. H., M. A. R. Garofalo, and I. C. Kettelhut.** Increased sympathetic activity in rat white adipose tissue during prolonged fasting. *Am. J. Physiol*. 272 (*Regulatory Integrative Comp. Physiol*. 41): R656–R661, 1997.
35. **Minokoshi, Y., M. Saito, and T. Shimazu.** Sympathetic denervation impairs responses of brown adipose tissue to VMH stimulation. *Am. J. Physiol*. 251 (*Regulatory Integrative Comp. Physiol*. 20): R1005–R1008, 1986.
36. **Morin, L. P., and J. Blanchard.** Organization of the hamster paraventricular hypothalamic nucleus. *J. Comp. Neurol*. 332: 341–357, 1993.
37. **Niijima, A., F. Rohner-Jeanrenaud, and B. Jeanrenaud.** Effects of cold stimulation on the efferent discharges of nerves innervating interscapular brown adipose tissue in the rat. *Neurosci. Lett*. 9: 59, 1982.
38. **Niijima, A., F. Rohner-Jeanrenaud, and B. Jeanrenaud.** Role of ventromedial hypothalamus on sympathetic efferents of

brown adipose tissue. *Am. J. Physiol*. 247 (*Regulatory Integrative Comp. Physiol*. 16): R650–R654, 1984.
39. **Paxinos, G., and C. Watson.** *The Rat Brain in Stereotaxic Coordinates*. Orlando, FL: Academic Press, 1986.
40. **Perkins, M. N., N. J. Rothwell, M. J. Stock, and T. W. Stone.** Activation of brown adipose tissue thermogenesis by the ventromedial hypothalamus. *Nature* 289: 401–402, 1981.
41. **Rothwell, N. J., and M. J. Stock.** Neural regulation of thermogenesis. *Trends Neurosci*. 5: 124–126, 1982.
42. **Ruby, N. F., N. Ibuka, B. M. Barnes, and I. Zucker.** Suprachiasmatic nuclei influence torpor and circadian temperature rhythms in hamsters. *Am. J. Physiol*. 257 (*Regulatory Integrative Comp. Physiol*. 26): R210–R215, 1989.
43. **Saito, M., Y. Minokoshi, and T. Shimazu.** Brown adipose tissue after ventromedial hypothalamic lesions in rats. *Am. J. Physiol*. 248 (*Endocrinol. Metab*. 11): E20–E25, 1985.
44. **Sakaguchi, T., K. Arase, J. S. Fisler, and G. A. Bray.** Effect of starvation and food intake on sympathetic activity. *Am. J. Physiol*. 255 (*Regulatory Integrative Comp. Physiol*. 24): R284–R288, 1988.
45. **Sakaguchi, T., and G. A. Bray.** Ventromedial hypothalamic lesions attenuate responses of sympathetic nerves to carotid arterial infusions of glucose and insulin. *Int. J. Obes*. 14: 127–134, 1990.
46. **Sakaguchi, T., M. Takahashi, and G. A. Bray.** Diurnal changes in sympathetic activity: relation to food intake and to insulin injection into the ventromedial or suprachiasmatic nucleus. *J. Clin. Invest*. 32: 282–286, 1988.
47. **Schramm, L. P., A. M. Strack, K. B. Platt, and A. D. Loewy.** Peripheral and central pathways regulating the kidney: a study using pseudorabies virus. *Brain Res*. 616: 251–262, 1993.
48. **Seydoux, J., F. Rohner-Jeanrenaud, F. Assimacopoulos-Jeannet, B. Jeanrenaud, and L. Girardier.** Functional disconnection of brown adipose tissue in hypothalamic obesity in rats. *Pflügers Arch*. 380: 1–4, 1981.
49. **Seydoux, J., E. R. Tribollet, and F. Bouillaud.** Effectiveness of surgical denervation of interscapular brown adipose tissue in the rat: further observations. In: *Thermal Physiology*, edited by J. R. S. Hales. New York: Raven, 1984, p. 197–199.
50. **Shibata, M., M. Iriki, J. Arita, T. Kiyohara, T. Nakashima, S. Miyata, and T. Matsukawa.** Procaine microinjection into the lower midbrain increases brown fat and body temperatures in anesthetized rats. *Brain Res*. 716: 171–179, 1996.
51. **Strack, A. M., and A. D. Loewy.** Pseudorabies virus: a highly specific transneuronal cell body marker in the sympathetic nervous system. *J. Neurosci*. 10: 2139–2147, 1990.
52. **Strack, A. M., W. B. Sawyer, J. H. Hughes, K. B. Platt, and A. D. Loewy.** A general pattern of CNS innervation of the sympathetic outflow demonstrated by transneuronal pseudorabies viral infections. *Brain Res*. 491: 156–162, 1989.
53. **Strack, A. M., W. B. Sawyer, K. B. Platt, and A. D. Loewy.** CNS cell groups regulating the sympathetic outflow to adrenal gland as revealed by transneuronal cell body labeling with pseudorabies virus. *Brain Res*. 491: 274–296, 1989.
54. **Takahashi, A., and T. Shimazu.** Hypothalamic regulation of lipid metabolism in the rat: effect of hypothalamic stimulation on lipogenesis. *J. Auton. Nerv. Syst*. 6: 225–235, 1982.
55. **Ter Horst, G. J., R. W. M. Hautvast, M. J. L. De Jongste, and J. Korf.** Neuroanatomy of cardiac activity-regulating circuitry: a transneuronal retrograde viral labeling study in the rat. *Eur. J. Neurosci*. 8: 2029–2041, 1996.
56. **Thornhill, J., and I. Halvorson.** Brown adipose tissue thermogenic responses of rats induced by central stimulation: effect of age and cold acclimation. *J. Physiol. (Lond.)* 426: 317–333, 1990.
57. **Thornhill, J., and I. Halvorson.** Differences in brown adipose tissue thermogenic responses between Long-Evans and Sprague-Dawley rats. *Am. J. Physiol*. 263 (*Regulatory Integrative Comp. Physiol*. 32): R59–R69, 1992.
58. **Thornhill, J., and I. Halvorson.** Intrascapular brown adipose tissue (IBAT) temperature and blood flow responses following ventromedial hypothalamic stimulation to sham and IBAT-denervated rats. *Brain Res*. 615: 289–294, 1993.
59. **Thornhill, J., A. Jugnauth, and I. Halvorson.** Brown adipose tissue thermogenesis evoked by medial preoptic stimulation is mediated via the ventromedial hypothalamic nucleus. *Can. J. Physiol. Pharmacol*. 72: 1042–1048, 1994.
60. **Van der Tuig, J. G., J. Kerner, and D. R. Romsos.** Hypothalamic obesity, brown adipose tissue, and sympathoadrenal activity in rats. *Am. J. Physiol*. 248 (*Endocrinol. Metab*. 11): E607–E617, 1985.
61. **Van der Tuig, J. G., A. W. Knehans, and D. R. Romsos.** Reduced sympathetic nervous system activity in rats with ventromedial hypothalamic lesions. *Life Sci*. 30: 913–920, 1982.
62. **Young, J. B., E. Saville, N. J. Rothwell, M. J. Stock, and L. Landsberg.** Effect of diet and cold exposure on norepinephrine turnover in brown adipose tissue of the rat. *J. Clin. Invest*. 69: 1061–1071, 1982.
63. **Youngstrom, T. G., and T. J. Bartness.** Catecholaminergic innervation of white adipose tissue in the Siberian hamster. *Am. J. Physiol*. 268 (*Regulatory Integrative Comp. Physiol*. 37): R744–R751, 1995.